TECHNICAL NOTE

On the effect of the Prandtl number on the onset of Bénard convection

J. L. Lage, A. Bejan and J. Georgiadis
Department of Mechanical Engineering and Materials Science, Duke University, Durham, NC, USA

This note summarizes the results of a numerical study designed to question (i.e., refute or validate) Chao *et al.*'s[1] and Bertin and Ozoe's[2] conclusion that the critical Rayleigh number increases substantially as the Prandtl number becomes very small. The numerical method is based on the finite-difference control volume formulation and the complete equations for two-dimensional (2-D) time-dependent flow. The present results show that the lowest attainable Rayleigh number for numerically simulated convection increases as Pr decreases below 0.1. These results also extend the Prandtl number domain of the observations down to $Pr = 10^{-4}$ and indicate that the natural shape of a single roll in this Pr range is approximately square. The discrepancy between these observations and the constant $Ra_c = 1{,}707.8$ of the linear stability analysis is attributed to the extrapolation method on which the numerical convection-onset Ra data[1,2] were based. It is shown that the numerical results agree with the linear stability constant $Ra_c = 1{,}707.8$ and Schlüter *et al.*'s[9] small amplitude perturbation analysis.

Keywords: Bénard convection; critical Rayleigh number; Prandtl number effect

Introduction

Eight years ago, Chao *et al.*[1] reported that the critical Rayleigh number (Ra_c) for the onset of Bénard convection increases substantially when the Prandtl number decreases to values as low as 0.01. A few years later, Bertin and Ozoe[2] drew a similar conclusion in simulations based on the finite-element method and the steady-state version of the governing equations. Bertin and Ozoe's steady-state solutions covered the Pr range of 0.003–1,000.

The claim that Ra_c should increase as Pr decreases runs counter to the classical view, which is that Ra_c is a constant independent of Pr. According to the method of linear stability analysis, that constant is 1,707.8 for a fluid layer held between two rigid (no-slip) horizontal walls. The constant-Ra_c conclusion is an integral part of all modern natural convection monographs. For example, Turner[3] specifically states that "the Prandtl number ν/α does not enter into this time-independent problem." And, in the latest treatise on hydrodynamic stability, Drazin and Reid[4] stress that "... the critical conditions, but not the rate of growth or damping, are independent of the Prandtl number." Finally, Busse's[5] tableau of the known transitions in Bénard convection (Figure 5 in his paper) shows a straight horizontal line (i.e., a Pr-independent Ra_c) for the boundary between "no motion" and "steady rolls."

The obvious conflict between these two views is a source of controversy, not because of the impassioned debate that it might generate but because of the silence with which it has been received in the published literature. A study of the post-1982 Annual Science Citation Index shows no reports that question the conclusions reached by Chao *et al.*[1] and Bertin and Ozoe.[2] The only comment found was offered by Proctor,[6] who in a review of the book in which Reference 1 appeared, rejected Chao *et al.*'s conclusion that the critical Rayleigh number varies with the Prandtl number.

The first objective of the numerical work described in this note was to question (refute or validate) the numerical conclusion that the lowest convection Rayleigh number increases dramatically as Pr decreases. Intentionally, the numerical method chosen for the present work (control volume formulation, complete governing equations) differs from the methods utilized in References 1 and 2. An additional objective was to extend the numerical study of the convection onset to Prandtl numbers as low as 10^{-4}, i.e., to Pr values more than one order of magnitude lower than those considered in References 1 and 2. Another objective was to determine the natural aspect ratio of the cross section of a single two-dimensional (2-D) roll near the onset of Bénard convection in low Prandtl number fluids.

Method

The conservation equations for 2-D natural convection in a Boussinesq fluid are

$$\frac{\partial U}{\partial X}+\frac{\partial V}{\partial Y}=0 \tag{1}$$

$$\frac{\partial U}{\partial \tau}+U\frac{\partial U}{\partial X}+V\frac{\partial U}{\partial Y}=-\frac{\partial P}{\partial X}+\left(\frac{\mathrm{Pr}}{\mathrm{Ra}}\right)^{1/2}\cdot\nabla^2 U \tag{2}$$

$$\frac{\partial V}{\partial \tau}+U\frac{\partial V}{\partial X}+V\frac{\partial V}{\partial Y}=-\frac{\partial P}{\partial Y}+\left(\frac{\mathrm{Pr}}{\mathrm{Ra}}\right)^{1/2}\cdot\nabla^2 V+\theta \tag{3}$$

$$\frac{\partial \theta}{\partial \tau}+U\frac{\partial \theta}{\partial X}+V\frac{\partial \theta}{\partial Y}=(\mathrm{Ra}\,\mathrm{Pr})^{-1/2}\cdot\nabla^2\theta \tag{4}$$

This dimensionless formulation is based on Figure 1 and the

Address reprint requests to Professor Bejan at the Department of Mechanical Engineering and Materials Science, Duke University, Durham, NC 27706, USA.

Received 25 January 1990; accepted 29 June 1990

© 1991 Butterworth-Heinemann

following definitions:

$$(X, Y)=\frac{(x, y)}{H} \qquad (U, V)=\frac{(u, v)}{(\alpha/H)(\mathrm{Ra\,Pr})^{1/2}} \tag{5}$$

$$\tau=\frac{\alpha t}{H^2}(\mathrm{Ra\,Pr})^{1/2} \qquad \theta=\frac{T-(T_h+T_c)^{1/2}}{T_h-T_c} \tag{6}$$

$$P=\frac{H^2(p+\rho g y)}{\rho\alpha^2 \mathrm{Ra\,Pr}} \qquad \mathrm{Pr}=\frac{\nu}{\alpha} \qquad \mathrm{Ra}=\frac{g\beta H^3(T_h-T_c)}{\alpha\nu} \tag{7}$$

We can rewrite the energy equation, Equation 4, in terms of the convection-induced correction to the temperature field, $\phi(X, Y, \tau)$:

$$\phi=\theta-\theta_c \tag{8}$$

in which θ_c represents the well-known pure conduction temperature distribution in the absence of fluid motion, or

$$\theta_c=\tfrac{1}{2}-Y \tag{9}$$

The resulting form of the energy equation is

$$\frac{\partial\phi}{\partial\tau}+U\frac{\partial\phi}{\partial X}+V\frac{\partial\phi}{\partial Y}=(\mathrm{Ra\,Pr})^{-1/2}\cdot\nabla^2\phi+V \tag{10}$$

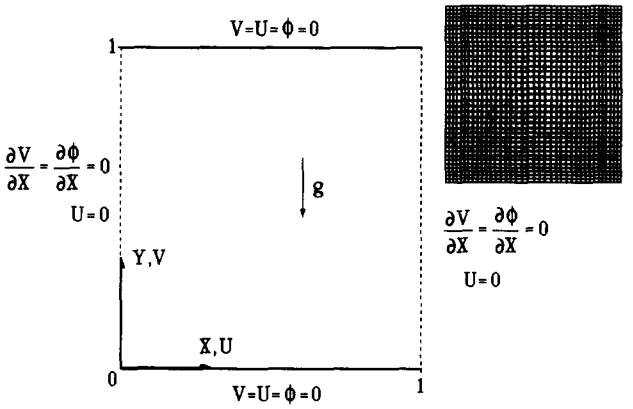

Figure 1 Computational domain and boundary conditions for a 2-D roll with square cross section

Equations 1–3 and 10 were subject to the boundary conditions listed in Figure 1. The square domain represents the cross section of one of the 2-D rolls known to form during the onset of convection between the differentially heated horizontal walls. The validity of the square-roll assumption in the low Pr range was demonstrated numerically in the wide-layer simulations (as presented later in Figure 5). The square shape of the domain was held fixed. The boundary conditions imposed on the vertical sides of the square state that the flow is purely vertical, with zero shear, and that the vertical sides are adiabatic.

The main requirement in the selection of the present numerical method was the need to use a method that differed substantially from that of Bertin and Ozoe[2] (finite-element, steady-state version of the governing equations). This requirement was met by the control-volume finite-difference method described by Patankar.[7] The square domain was divided into a large number of square control volumes of various sizes, and Equations 1–3 and 10 were integrated over each control volume. The flux terms were made discrete by use of the power-law method. The SIMPLE algorithm was used in order to solve the control-volume conservation statements and the pressure-correction equation that results from imposing Equation 1. The time derivatives were approximated by means of first-order forward differences, which led to a system of algebraic equations implicit in time. This system was solved using the Tri-Diagonal-Matrix-Algorithm in a line-by-line manner, by sweeping the entire domain in both directions for each variable.

The initial condition used in all the numerical runs was the quiescent, pure conduction state:

$$U=V=\phi=0 \qquad \text{at } \tau=0 \tag{11}$$

The initial temperature distribution was perturbed by assigning a horizontal gradient to the temperatures in the mid-height plane:

$$\phi=\tfrac{1}{2}Pr(\tfrac{1}{2}-X) \qquad \text{at } Y=\tfrac{1}{2} \text{ and } \tau=0 \tag{12}$$

The reason for using the Prandtl number as a factor in Equation 12 is that the Pr has opposing effects on the energy and momentum equations. As Pr decreases, the nonlinear (convection) terms become less significant in Equation 10, while the nonlinear (inertia) terms gain in importance in the momentum equations, Equations 2 and 3. Consequently, in the low Prandtl

Notation

B	Function of Prandtl number
g	Gravitational acceleration
H	Vertical dimension of fluid layer
i	Iteration order
k	Thermal conductivity
l	Width of a single roll
L	Width of numerical domain in Figures 4 and 5
$\mathrm{Nu_b}$	Bottom-wall overall Nusselt number
$\mathrm{Nu_m}$	Mid-height overall Nusselt number
p	Pressure
P	Dimensionless pressure
Pr	Prandtl number
q''_{avg}	Average bottom-wall heat flux
Ra	Rayleigh number
$\mathrm{Ra_c}$	Critical Rayleigh number, $\mathrm{Ra_c}=1707.8$
Ra′	Extrapolated convection-onset Rayleigh number, Figure 3
s_j	Spatial location of the grid line
t	Time
T	Temperature
T_c	Temperature of cold (top) wall
T_h	Temperature of hot (bottom) wall
u, v	Velocity components
U, V	Dimensionless velocity components
x, y	Cartesian coordinates
X, Y	Dimensionless Cartesian coordinates

Greek symbols

α	Thermal diffusivity
α_s	Rate of grid stretching
β	Coefficient of volumetric thermal expansion
Δ	Spacing of the two grid lines nearest the boundary
θ	Dimensionless temperature
θ_c	Pure conduction dimensionless temperature distribution
ν	Kinematic viscosity
ρ	Density
τ	Dimensionless time
ϕ	Convection correction to the dimensionless temperature distribution

number range of this study, convergence of the numerical solution is sensitive to the strength of the flow field (see the last term, V, in Equation 10). Smaller velocities improved convergence at progressively lower Prandtl numbers; therefore the temperature disturbance, Equation 12, was tailored so that it decreased with Pr.

The relaxation factors for the momentum and energy equations varies from 0.90 to 0.98. These relatively high values were needed because of the extremely weak flow that persists at the lowest Rayleigh numbers where convection was present.

The convergence of the numerical solution was monitored both locally and globally. The max-norm value was used for the velocity components (U, V) and the temperature correction function (ϕ). The global parameter was the overall Nusselt number based on the heat flux averaged over the bottom wall:

$$\mathrm{Nu_b}=\frac{q''_{\mathrm{avg}}H}{k(T_\mathrm{h}-T_\mathrm{c})}=-\int_0^1\left(\frac{\partial\theta}{\partial Y}\right)_{Y=0}dX \tag{13}$$

The convergence criteria at each time step were

$$\mathrm{MAX}\left|\frac{(U,V,\phi)^{i+1}-(U,V,\phi)^i}{(U,V,\phi)^i}\right|<10^{-3} \tag{14}$$

$$\frac{\mathrm{Nu}_\mathrm{b}^{i+1}-\mathrm{Nu}_\mathrm{b}^i}{\mathrm{Nu}_\mathrm{b}^i}<10^{-6} \tag{15}$$

in which i and $i+1$ are two consecutive iterations at the same time step. In the steady state, the difference between the bottom Nusselt number ($\mathrm{Nu_b}$) and the mid-height Nusselt number

$$\mathrm{Nu_m}=\int_0^1\left[(\mathrm{Ra\,Pr})^{1/2}V\theta-\frac{\partial\theta}{\partial Y}\right]_{Y=\frac{1}{2}}dX \tag{16}$$

was less than 10^{-5}. The $\mathrm{Nu_m}$ parameter is a dimensionless measure of the total heat transfer rate (conduction and convection) through the horizontal mid-plane of the square roll.

The grid was slightly nonuniform, with smaller control volumes placed near the four boundaries:

$$s_{j+1}=s_j+\alpha_\mathrm{s}^j\Delta \tag{17}$$

where s_j is the spatial location of the jth grid line (s_j is measured away from the boundary) and α_s and Δ are the rate of grid stretching and the spacing of the two grid lines nearest the boundary, respectively. The choice of 40×40 grid with $\alpha_\mathrm{s}=1.0296$ and $\Delta=0.02$ (see the reduced detail of Figure 1) was based on the accuracy test illustrated in Figure 2. We found that a more nonuniform grid (larger α_s) does not reveal any new information, because near the convection onset the flow fills the entire square.

For each Pr case, the Rayleigh number was decreased to the lowest level allowed by our computational means. This difficulty was caused not only by the progressively low rate of viscous damping (in spite of Equation 12), but also by the overall Nusselt number taking on values very close to 1. The simulation of Ra cases below the lowest Ra's listed in Table 1 would have required considerably more stringent (i.e., computationally prohibitive) convergence criteria than the ones listed in Equations 14 and 15.

Numerical results

Table 1 summarizes all the steady-state values obtained for the overall Nusselt number. In order to see whether these $\mathrm{Nu_b}$ values agree with Bertin and Ozoe's,[2] we used their method of correlating these data for the purpose of finding the "extrapolated critical" Rayleigh number Ra′. This number is shown at the bottom of each block of Pr values in Table 1. It was obtained exactly as in Reference 2 by correlating the numerical $\mathrm{Nu_b}$ data in accordance with Malkus and Veronis'[8] equation,

$$\mathrm{Nu_b}=1+\left[1-\frac{\mathrm{Ra'(Pr)}}{\mathrm{Ra}}\right]B(\mathrm{Pr}) \tag{18}$$

and by setting $\mathrm{Nu_b}=1$. Figure 3 shows that the present extrapolated Ra′ values agree well with those of Bertin and Ozoe.[2] The maximum difference between the two sets is less

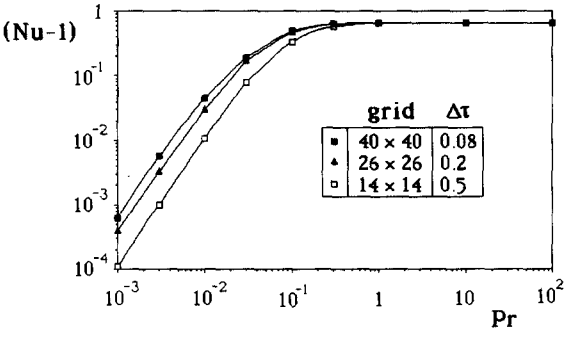

Figure 2 The effect of grid size on numerical accuracy (Ra = 3,000)

Table 1 Numerical results for the overall Nusselt number in the vicinity of the onset of Bénard convection

Pr = 0.0001		Pr = 0.0003		Pr = 0.001		Pr = 0.003		Pr = 0.01	
Ra	$\mathrm{Nu_b}$	Ra	$\mathrm{Nu_b}$	Ra	$\mathrm{Nu_b}$	Ra	$\mathrm{Nu_b}$	Ra	$\mathrm{Nu_b}$
3850	1.000030	3450	1.000155	3100	1.000946	2900	1.005433	2700	1.030209
3800	1.000021	3400	1.000119	3000	1.000634	2700	1.003087	2500	1.020762
3750	1.000012	3350	1.000083	2950	1.000470	2600	1.001779	2300	1.009672
3700	1.000002	3300	1.000046	2900	1.000300	2500	1.000366	2200	1.003370
Ra′ = 3,685.7		Ra′ = 3,240.8		Ra′ = 2,815.3		Ra′ = 2,475.3		Ra′ = 2,150.0	

Pr = 0.03		Pr = 0.1		Pr = 0.3		Pr = 1		Pr = 10		Pr = 100	
Ra	$\mathrm{Nu_b}$	Ra	$\mathrm{Nu_b}$	Ra	$\mathrm{Nu_b}$	Ra	$\mathrm{Nu_b}$	Ra	$\mathrm{Nu_b}$	Ra	$\mathrm{Nu_b}$
2300	1.085451	2300	1.289227	2300	1.392743	2300	1.395814	2300	1.395805	2300	1.395802
2100	1.047418	2100	1.206273	2100	1.284556	2100	1.287064	2100	1.287060	2100	1.287059
2000	1.025551	1900	1.105807	1900	1.153594	1900	1.154012	1900	1.154011	1900	1.154010
1900	1.013780	1800	1.047201	1800	1.077199	1800	1.077998	1800	1.077997	1800	1.077997
Ra′ = 1,894.6		Ra′ = 1,726.8		Ra′ = 1,709.1		Ra′ = 1,708.8		Ra′ = 1,708.8		Ra′ = 1,708.8	

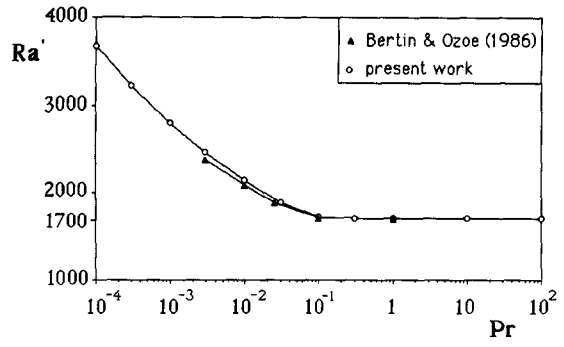

Figure 3 The Pr effect on the extrapolated Rayleigh number for the onset of convection

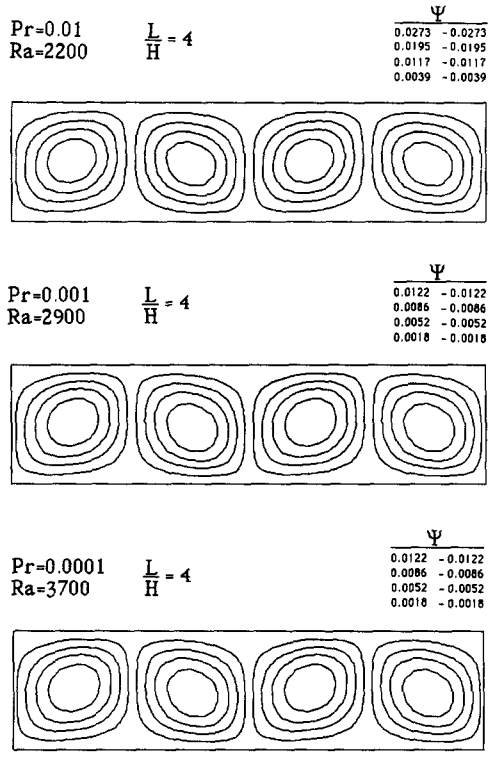

Figure 4 The natural square shape of the cross section of each 2-D roll

than 3 percent. The present Ra′ calculations extend down to $Pr = 10^{-4}$, whereas Bertin and Ozoe could not obtain converged steady-state solutions below $Pr = 0.003$.

In References 1 and 2, the extrapolated Ra′ was viewed the same as the critical Rayleigh number for the onset of convection, Ra_c. It would be tempting to reconcile the empirical conclusion that Ra′ = function (Pr) with the constant-Ra_c dictum of hydrodynamic stability theory by arguing that the square roll (Figure 1) is an unrealistic assumption in the low Prandtl number range. This possibility became the subject of an additional set of numerical simulations in a very shallow domain in which the width of each roll was not fixed by means of boundary conditions. The Rayleigh number was decreased as much as possible for the purpose of observing the natural number and shape of the rolls that persist.

Figure 4 shows the flow pattern in the Pr range of 10^{-2} to 10^{-4}. In each case, the Ra value is the lowest for which convection was detected in the numerical experiments reviewed in Table 1. The boundary conditions on the vertical sides of the shallow layer of Figure 4 were the same as those on the sides of the square in Figure 1. The grid was 104×26, i.e., 26×26 for each fourth (square) of the shallow layer. This grid is coarser than the 40×40 grid used for the square domain (Figure 2). The computational time would have been prohibitive had we tried a grid of the same fineness (40×40 per square) for the shallow layer.

In Figure 4, the numbers listed next to each set of streamlines represent the dimensionless stream function Ψ, for which

$$U = \frac{\partial \Psi}{\partial y} \quad \text{and} \quad V = -\frac{\partial \Psi}{\partial X} \tag{19}$$

The negative and positive Ψ values indicate clockwise and counterclockwise rolls, respectively. The largest absolute Ψ value corresponds to the streamline closest to the center of the roll. These stream-function values are virtually identical to the ones calculated using the square domain of Figure 1.

The streamline patterns of Figure 4 support the assumption that the natural shape of the near-critical roll is square in the low Pr range of this numerical study. The natural shape of the near-critical roll was pursued further in Figure 5, in which Pr and Ra were held constant while the width of the numerical domain was increased. In association with the middle part of Figure 4, Figure 5 shows what happens for successive L/H values of 4, 4.5, and 5.

The number of cells increases from four (Figure 4) to five (Figure 5), as L/H increases from 4 to 4.5. For the width/height ratio of a single roll, l/H, at $Pr = 10^{-3}$ the natural l/H of the roll has a value between 1 and 0.9. This finding is approximated well by the $l/H = 1$ assumption on which the data of Table 1 are based.

Conclusions

We have shown by a different method that the actual numerical results reported in References 1 and 2 are correct. By themselves, these results are useful because they show that simulating near-critical Bénard convection numerically near $Ra = 1{,}707.8$ when the Prandtl number is less than 0.1 is very difficult.

The divergence between the Ra′(Pr) curve of Figure 3 and the Ra_c constant of the linear stability analysis can only be attributed to the extrapolation method[1,2] that produced the

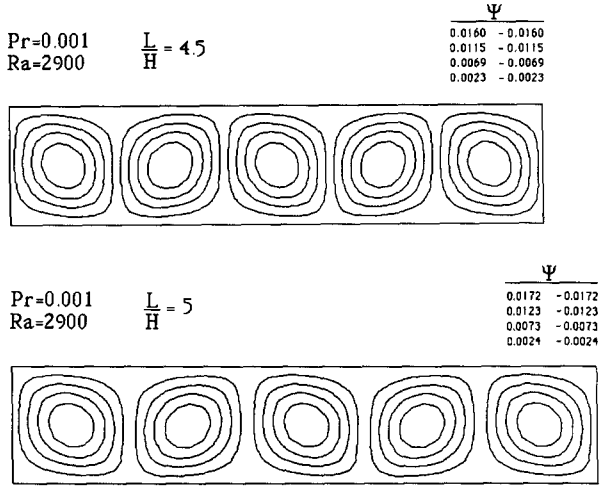

Figure 5 Multiplication of rolls as the layer width increases at constant Pr and Ra

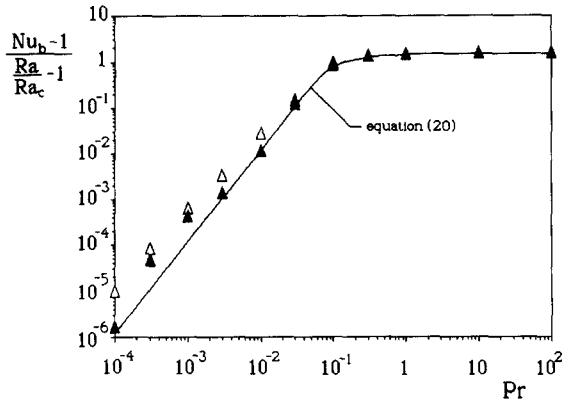

Figure 6 Agreement between the present results and Schlüter *et al.*'s[9] asymptotic theory for $Ra \to Ra_c$, with $Ra_c = 1{,}707.8$

Ra′ values of Table 1, i.e., to the fact that Ra′ is not Ra_c. Indeed, Schlüter *et al.*'s[9] small amplitude perturbation analysis showed that close to the onset of 2-D rolls the overall Nusselt number behaves as

$$Nu_b = 1 + \left(\frac{Ra}{Ra_c} - 1\right)(0.69942 - 0.00472\,Pr^{-1} + 0.00832\,Pr^{-2})^{-1} \tag{20}$$

in which $Ra_c = 1{,}707.8$. This asymptotic theory is supported by the Nu_b data developed in this study. Figure 6 shows the Nu_b curve given by Equation 20, next to the lowest Ra data of each of the Pr blocks of Table 1. Specifically, the black triangles correspond to the lowest Ra case simulated numerically, and the white triangles correspond to the second-lowest Ra case. The agreement between Equation 20 and the numerical Nu_b data is not as good in the range $Pr \leq 10^{-3}$ because of the convergence difficulties noted in the Method section. This agreement improves visibly as we shift from the white triangles to the black triangles, i.e., as the Rayleigh number decreases. The agreement is surprisingly good in view of Clever and Busse's[10] earlier conclusion that Equation 20 holds asymptotically when the excess Rayleigh number $(Ra - Ra_c)$ is less than $O(10)$. In the case of the triangles of Figure 6, the excess Rayleigh number is $O(10^2)$ and larger.

It is important to discuss our results in juxtaposition with the work of Clever and Busse.[11,12] Recent numerical simulations[11] show that the transition from thermal convection in the form of rolls to traveling wave convection occurs at $Ra = 1{,}854$ in the limit of $Pr \to 0$. This bifurcation corresponds to the oscillatory instability that gives rise to wavy distortions of the convection rolls that travel along the axis of the rolls. This is a three-dimensional (3-D) field that was not studied in the present work. A method to suppress this 3-D motion by using magnetic fields has been explored by Busse and Clever.[12]

We close by commenting on the validity of Equation 18, which was crucial in References 1 and 2. The power integral method of Malkus and Veronis[8] is known to give up to 10 percent inaccuracies in Nusselt number. Consequently, Equation 18 is useful only for crude approximations. Equation 20, which contradicts Equation 18 as far as Ra dependence is concerned, is the correct asymptotic formula. Its usefulness as $Pr \to 0$ is limited because it behaves as

$$Nu - 1 \sim (Ra - Ra_c)Pr^2 \tag{21}$$

Expression 21 shows that the departure of Nu above the conduction level $(Nu = 1)$ exceeds the practical numerical tolerances as Pr decreases.

Acknowledgment

Most of the numerical work was done on the IBM 3081 computer of the Triangle Universities Computation Center located in the Research Triangle Park, North Carolina. Some cases were run at the Cornell National Supercomputer Facilities (IBM 3090 600-E), using a vectorized version of the code.

References

1 Chao, P., Churchill, S. W., and Ozoe, H. The dependence of the critical Rayleigh number on the Prandtl number. *Convection Transport and Instability Phenomena* (J. Zierep and H. Oertel Eds.) G. Braun, Karlsrühe, FRG, 1982, 55–70

2 Bertin, H. and Ozoe, H. Numerical study of two-dimensional convection in a horizontal fluid layer heated from below, by finite-element method: influence of Prandtl number. *Int. J. Heat Mass Transfer*, 1986, **29**, 439–449

3 Turner, J. S. *Buoyancy Effects in Fluids*. Cambridge University Press, Cambridge, England, 1973, 210

4 Drazin, P. G. and Reid, W. H. *Hydrodynamic Stability*. Cambridge University Press, Cambridge, England, 1981, 50

5 Busse, F. H. Non-linear properties of thermal convection. *Rep. Prog. Phys.*, 1978, **41**, 1929–1967

6 Proctor, M. R. E. Book review. *J. Fluid Mech.*, 1983, **137**, 462–463 (review of ref. 1)

7 Patankar, S. V. *Numerical Heat Transfer and Fluid Flow*. Hemisphere, Washington, D.C., 1980

8 Malkus, W. V. R. and Veronis, G. Finite amplitude cellular convection. *J. Fluid Mech.*, 1958, **4**, 225–260

9 Schlüter, A., Lortz, D., and Busse, F. On the stability of steady finite amplitude convection. *J. Fluid Mech.*, 1965, **23**, 129–144

10 Clever, R. M. and Busse, F. H. Low-Prandtl number convection in a layer heated from below. *J. Fluid Mech.*, 1981, **102**, 61–74

11 Clever, R. M. and Busse, F. H. Convection at very low Prandtl numbers. *Phys. Fluids A*, 1990, **2**(3), 334–339

12 Busse, F. H. and Clever, R. M. Traveling-wave convection in the presence of a horizontal magnetic field. *Physical Rev. A*, 1989, **40**(4), 1954–1961